Supporting Information

Renner and Weibel 10.1073/pnas.1015757108

SI Materials and Methods

Bacterial Strains and Culture. *Escherichia coli* K-12 strains MG1655 (CGSC 8237), UE54 (MG1655 lpp-2 Δara714 rcsF::mini-Tn10cam ΔpgsA::FRT-kan-FRT) (1), and JW 1241 Δcls (2) were used for the experiments described in this paper. Bacteria were grown in LB liquid medium (10 g/L tryptone, 5 g/L yeast extract, 10 g/L NaCl) at 37 °C; 25 μg/mL of kanamycin was added to growth medium for strain JW 1241 Δcls. LB medium containing 1.5% (wt/vol) LB agar (Difco) was used for the growth of colonies of *E. coli* MG1655 and JW 1241 Δcls. Tryptone, yeast extract, peptone, and bacteriological agar were from Becton Dickinson. Sodium chloride was from Fisher Scientific. Petri dishes were from Becton Dickinson. For the localization study of *E. coli* MinD, we purified the plasmid from strain *E. coli* pFX40 (P_{lac}::*yfp-minD min E*) (3, 4) and transformed it into *E. coli* MG1655 and JW 1241 Δcls cells (5). We further used the plasmid pEGFP to express cytoplasmic eGFP in *E. coli* MG1655 constitutively (eGFP ORF expressed via the Lac promoter from Clontech). The plasmids pFX40 and pEGFP (50 μg/mL) conferred ampicillin resistance to cells.

Preparation of Substrates. We designed patterns of microchambers in CleWin (Delta Mask) and used these designs to fabricate a chrome mask. The microchambers consisted of six repetitive features that had a length of ∼3–4 μm and a radius at the caps ranging from 0.48–1.5 μm, corresponding to curvatures of 2.08–0.67 μm^{-1}, respectively. We determined the curvature of the microchambers according to Fig. S4. We transferred the pattern from the mask into a layer of Shipley PR 1827 that was 3 μm thick using photolithography. The resulting master contained embossed features and was silanized for 8 h using a vapor of (tridecafluoro-1,1,2,2-tetrahydrooctyl)trichlorosilane (Gelest, Inc). We created the inverse pattern in polydimethylsiloxane (PDMS) (Sylgard 184 elastomer kit, Dow Corning) using a base-to-curing agent ratio of 10:1. We poured prepolymer on the master and cured it overnight at 60 °C (6). The resulting PDMS layer contained posts in bas-relief and was used as a stamp to emboss a layer of agarose.

A hot solution of 4% agarose (EM-2120, Omni-pur; EM Biosciences) was poured on the PDMS stamp oriented with the embossed features facing up and was cooled to 25 °C. The layer of agarose embossed with microchambers was excised with a scalpel, and 3 μL of a suspension of purified *E. coli* spheroplasts was added on the top surface of the agarose (microchambers facing up). During 2-min incubation the excess liquid was absorbed by the gel. Capillary pressure pulled the spheroplasts in the chambers; some spheroplasts remained on the agarose surface. We sealed the spheroplasts in the microchambers by placing a clean #1.5 glass coverslip (12-548-5g; Fisher Scientific) on top of the agarose.

Preparation of Giant Spheroplasts. We prepared giant spheroplasts of *E. coli* MG1655 (±pFX40) and *E. coli* JW 1241 Δcls (+pFX40) by modifying the procedure described by Martinac et al. (7) and Kuo et al. (8). In summary, a liquid culture of *E. coli* was grown overnight from a single colony, and a small aliquot (1:100 dilution) was used to inoculate modified LB liquid medium (10 g/L tryptone, 5 g/L yeast extract, 5 g/L NaCl). The culture was incubated at 37 °C with shaking at 200 rpm and grown to an absorbance of 0.5–0.7 (λ = 600 nm). The cell culture was diluted 1:10 in 4.5 mL of prewarmed modified LB medium containing 60 μg/mL cephalexin (C4895; Sigma Aldrich). We incubated the cells for 3–4 h at 37 °C with shaking at 200 rpm to grow cells into filaments. We began monitoring the length of cells after 3 h of growth. When cells reached an average length of ∼50 μm, the cells were harvested, and 1 mL of the cell suspension was pelleted at 3,000 × *g* for 1 min. The pellet was resuspended carefully in 500 μL of a 0.8-M sucrose solution by gently inverting the test tube several times. We added the following solutions to the aliquot of cells (with immediate mixing between additions): 30 μL 1 M Tris·HCl (pH 8.0), 24 μL 0.5 mg/mL lysozyme (∼20 μg/mL final concentration), 6 μL 5 mg/mL DNase (∼50 μg/mL final concentration), and 6 μL 125 mM EDTA-NaOH (pH 8.0) (∼1.3 mM final concentration). The mixture was incubated for 5–10 min at 25 °C, and 100 μL of STOP solution [10 mM Tris·HCl (pH 8), 0.7 M sucrose, 20 mM $MgCl_2$] was added to terminate the digestion.

We confirmed the formation of spheroplasts by optical microscopy.

Spheroplasts were aliquoted into tubes and used directly or were frozen on dry ice and stored at −80 °C. Frozen aliquots of spheroplasts were thawed slowly on ice before use. We labeled the spheroplasts with 400 nM nonyl acridine orange (NAO) (A7847; Sigma-Aldrich) for 55 min at 25 °C to visualize cardiolipin (CL) (9) followed by labeling for 5 min with 100 nM DAPI (D9564; Sigma-Aldrich) to observe DNA. Incubation of MG1655 for 3–4 h in medium containing 60 μg/mL cephalexin produced filamentous cells ∼50 μm long that we converted into spheroplasts with a mean diameter of 3.5 ± 0.95 μm (compare Fig. 1 and Fig. S1) (10).

A slightly modified procedure was applied to *E. coli* MG1655 and JW 1241 Δcls containing plasmid pFX40: A 5-mL overnight culture was grown from a single colony at 37 °C in LB liquid medium containing 50 μg/mL ampicillin (and 25 μg/mL kanamycin for JW 1241 Δcls) and 0.4% glucose. We diluted cells 1:100 in fresh liquid LB medium (containing ampicillin and glucose) and grew the culture at 30 °C to an absorbance of ∼0.5–0.7 (λ = 600 nm, ∼2.5 h). Then 1 mL of the culture was centrifuged, and the cell pellet was washed twice in LB medium containing ampicillin and glucose. The pellet was resuspended in 5 mL LB containing 50 μg/mL ampicillin, 60 μg/mL cephalexin, and 10 μM isopropyl-β-D-thio-galactoside (IPTG). Cells were grown at 30 °C, and the cell length was analyzed after 3 h. If the observed cells were less than ∼50 μm long, we checked the culture by microscopy every 30–60 min until they reached the desired length. To create spheroplasts, we used the procedure described previously. The distribution of MinD-YFP was analyzed directly after spheroplast formation, or the spheroplasts were incubated for 55 min with NAO (final concentration 400 nM) and DAPI for 5 min (final concentration 1 μg/mL) (compare Figs. S7 and S8).

To test the localization behavior in spheroplasts of a protein that is not supposed to associate with the bacterial membrane, we expressed cytoplasmic eGFP in *E. coli* MG1655 by induction with 10 μM IPTG. We followed the spheroplast preparation procedure explained above. An example of the localization behavior is given in Fig. S9. No localization of eGFP could be detected in dependence of the imposed curvature of the microchambers.

Microscopy and Image Analysis. We imaged spheroplasts on a Nikon TE2000 inverted microscope (Nikon Inc.) equipped with an Andor iXon EMCCD (Andor Technology). The fluorescent dyes were excited using a mercury lamp (EXFO Life Sciences) and the appropriate filters (DAPI: λ_{ex} = 355 nm/λ_{em} = 460 nm; NAO: λ_{ex} = 488 nm/λ_{em} = 628 nm; YFP: λ_{ex} = 500 nm/ λ_{em} =

535 nm). The raw data fluorescent images (16-bit, gray-value images) were merged with phase-contrast bright-field images of the micropatterns and analyzed using ImageJ (National Institutes of Health). We analyzed the data of the distribution of CL microdomains by extracting confined spheroplast images and plotting line scans over the entire cell. These line scans were fitted to a Gaussian function, and the position of the CL microdomain was determined by the center of the fit. Using this method for determining the position of CL, we analyzed all spheroplast images, determined the position of CL, and plotted the frequency. We performed 10 independent measurements from 10 independent spheroplasts preparations. For every feature at least 400 spheroplasts were analyzed.

Determination of Spheroplast Microchamber Topology. The pole length was estimated from electron microscopy images (Fig. S3). For example, spheroplasts confined in the rod-shaped microchambers can be divided into the following three regions: (*i*) a left segment that was 25% of the total length of the spheroplast; (*ii*) a middle segment that was the next 50% of the length of the spheroplast; and (*iii*) a right segment that was the remaining 25% of the total length of the spheroplast. This approach to segmenting spheroplasts seemed to be a reasonable estimate, because an *E. coli* cell has a length of ~2 μm (e.g., the cylindrical midsection of the cell is ~1 μm or 50% of its length), and the poles have a radius of ~0.5 μm (e.g., each 25% of the length of the cell). In the microchambers that we fabricated, the pole length—and the percentage of pole-segment length—becomes shorter as the curvature of the microchambers decreases.

Determination of Membrane Integrity and Confinement in Microchambers. The microchambers were designed so that the lateral curvature of the membrane imposed by the continuous surrounding wall would create a larger curvature than the vertical deformation of the spheroplast. In spherical microchambers (spheroplast curvature = 0.67 μm^{-1}), the curvature of spheroplast membranes in the vertical direction may, in principle, be larger than curvature in the lateral direction if the membranes are strongly bent and overlapping.

Spheroplast suspensions were heterogeneous and contained cellular debris (including fragments of cell membranes) that was difficult to remove and might complicate our analyses. We confined spheroplasts in microchambers and imaged them using phase-contrast microscopy. We developed a technique for selecting microchambers that contained spheroplasts confined without deformations in the membrane based on phase-contrast images. Although the phase-contrast images made it possible to discern some defects in membranes, we performed control experiments using FM 4–64 (T3166, Invitrogen) to label membranes of confined spheroplasts. We compared the phase-contrast and epifluorescence images of these spheroplasts. This analysis made it possible for us to select confined, intact, and nondeformed spheroplasts from phase-contrast images (Fig. S5). On the basis of the membrane shape, we selected uncompromised spheroplasts for the analysis of the CL localization.

We also used laser-scanning confocal microscopy (LSCM) (LSM510 Meta; Zeiss) to characterize spheroplast cell membranes. Rigorous analysis produced no obvious indication of membrane deformations in confined spheroplasts. We have included two 3D reconstructions of spheroplasts in microchambers to demonstrate these analyses; Movie S1 shows a confined spheroplast with a spherical shape; Movie S2 shows a confined spheroplast with a rod shape.

A potential issue that we considered was the mismatch in the volume of the microchambers and the spheroplasts, the latter of which are fabricated with a distribution of sizes (Fig. S1). To address this issue, we calculated the volume for each microchamber (Table S1). The volumes of the microchambers were calculated using a depth of 3.0 μm. The volume of the microchambers closely matches the volume of the spheroplasts. Spheroplasts with a diameter >4 μm have a volume larger than the microchambers, and their confinement may result in bulged, deformed, and bent regions of the membrane. We were able to avoid the analysis of these membranes using the method described above.

1. Shiba Y, et al. (2004) Activation of the Rcs signal transduction system is responsible for the thermosensitive growth defect of an *Escherichia coli* mutant lacking phosphatidylglycerol and cardiolipin. *J Bacteriol* 186:6526. 6535.
2. Baba T, et al. (2006) Construction of *Escherichia coli* K-12 in-frame, single-gene knockout mutants: The Keio collection. *Mol Syst Biol*, 2:2006.0008.
3. Shih YL, Fu X, King GF, Le T, Rothfield L (2002) Division site placement in *E. coli*: Mutations that prevent formation of the MinE ring lead to loss of the normal midcell arrest of growth of polar MinD membrane domains. *EMBO J* 21:3347–3357.
4. Shih YL, Le T, Rothfield L (2003) Division site selection in *Escherichia coli* involves dynamic redistribution of Min proteins within coiled structures that extend between the two cell poles. *Proc Natl Acad Sci USA* 100:7865–7870.
5. Hanahan D (1983) Studies on transformation of *Escherichia coli* with plasmids. *J Mol Biol* 166:557–580.
6. Xia Y, Whitesides GM (1998) Soft lithography. *Angew Chem Int Ed* 37:550–575.
7. Martinac B, Buechner M, Delcour AH, Adler J, Kung C (1987) Pressure-sensitive ion channel in *Escherichia coli*. *Proc Natl Acad Sci USA* 84:2297–2301.
8. Kuo MM-C, Saimi Y, Kung C, Choe S (2007) Patch clamp and phenotypic analyses of a prokaryotic cyclic nucleotide-gated K+ channel using *Escherichia coli* as a host. *J Biol Chem* 282:24294–24301.
9. Mileykovskaya E, Dowhan W (2000) Visualization of phospholipid domains in *Escherichia coli* by using the cardiolipin-specific fluorescent dye 10-N-nonyl acridine orange. *J Bacteriol* 182:1172–1175.
10. Onitsuka MO, Rikihisa Y, Maruyama HB (1979) Biochemical and topographical studies on *Escherichia coli* cell surface. IV. Giant spheroplast formation from a filamentous cell. *J Bacteriol* 138:567–574.

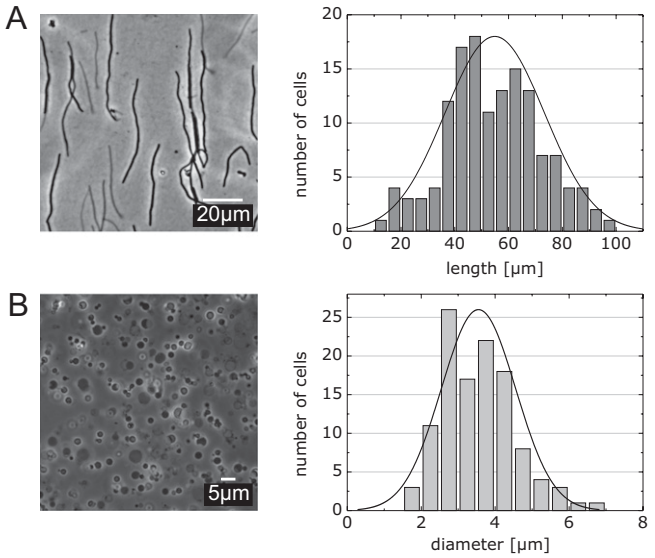

Fig. S1. (*A*) The distribution of lengths of filamentous *E. coli* cells after 4 h of filamentation. Mean length: 54 ± 18 µm; *n* = 142; data are from four independent experiments. (*B*) The distribution of the diameter of spheroplasts. Mean diameter: 3.55 ± 0.95 µm; *n* = 116; data are from four independent experiments.

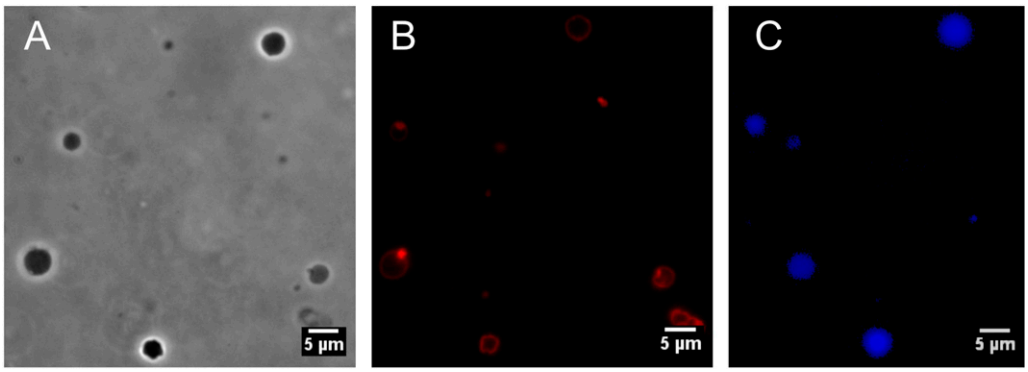

Fig. S2. Spheroplasts labeled with FM 4–64 and DAPI demonstrate the integrity of the inner membrane after the outer membrane and peptidoglycan are removed. The spheroplasts were labeled with FM4-64 (red) and DAPI (blue). (*A*) Phase-contrast microscopy image. (*B* and *C*) Epifluorescence images. The membrane is intact in two of the spheroplasts, and the presence of DNA confirms these membranes are continuous and intact.

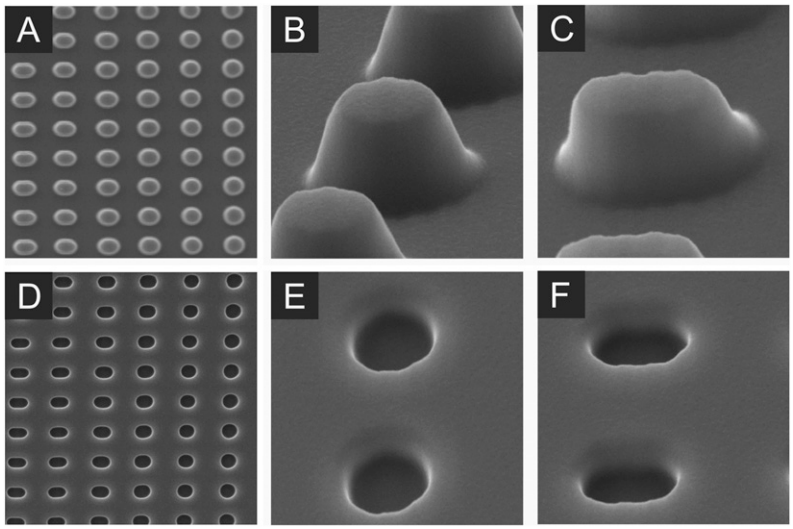

Fig. S3. Scanning electron microscopy images of the PDMS stamps used for embossing layers of agarose. (*A–C*) Images of structures in bas-relief on PDMS stamps. (*D–F*) Images of PDMS layers that were embossed using the stamps depicted in *A–C*; these images were created to demonstrate the shape of the resulting layer of agarose that was prepared for the experiments described in this manuscript. It was difficult to image embossed layers of agarose using SEM, so we used these PDMS layers as examples instead.

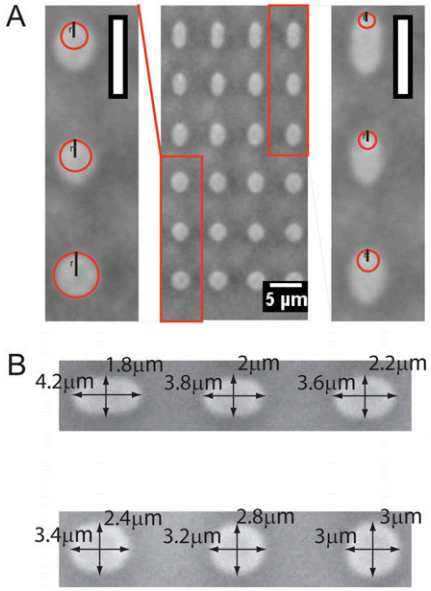

Fig. S4. The determination of the radius of curvature (*A*) and the dimension of the different microchambers (*B*).

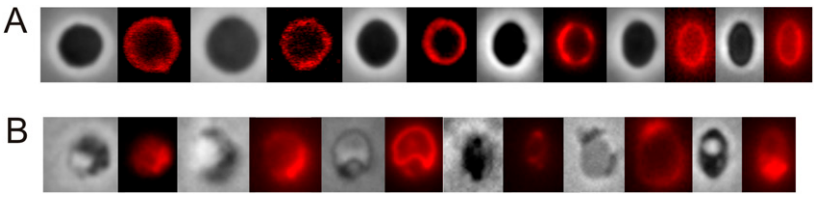

Fig. S5. Confined spheroplasts in microchambers. The spheroplasts were labeled with FM 4–64 and confined in microchambers. In each pair of images, the left image was acquired with phase-contrast microscopy; the image on the right was acquired with epifluorescence microscopy. The comparison of the membranes between the modes of imaging made it possible for us to select spheroplasts for analysis based on the phase-contrast image. (*A*) Based on the phase-contrast images, all these spheroplasts were acceptable for analysis of CL microdomain localization. (*B*) Based on the phase-contrast images, all these spheroplasts were unacceptable for analysis of CL microdomain localization; the deformation, disruption, and bending of the membranes are evident.

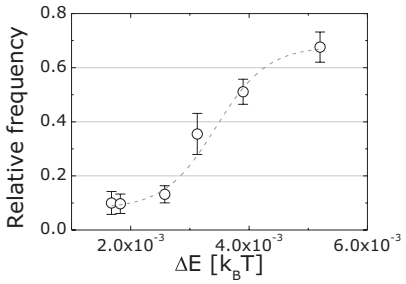

Fig. S6. Plot of frequency of CL microdomains vs. difference in elastic energy of the different curvatures of the microchambers for the localization of single CL molecules. The difference in elastic energy ΔE was calculated by the equation $\Delta E \approx \kappa\gamma_0\,\gamma_{lipid}\,A$ with κ the membrane bending stiffness ($\kappa \approx 25\ k_BT$), when γ_0 is the curvature of the microchambers, γ_{lipid} is the curvature of a single cardiolipin molecule ($\gamma_{lipid} \approx 0.1\ \text{nm}^{-1}$), and A is the surface area of a single cardiolipin molecule ($A \approx 1\ \text{nm}^2$) (1).

1. Mukhopadhyay R, Huang KC, Wingreen NS (2008) Lipid localization in bacterial cells through curvature-mediated microphase separation. *Biophys J* 95:1034–1049.

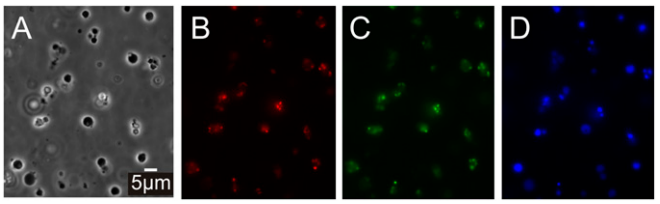

Fig. S7. MinD and CL localization in freshly prepared, freestanding spheroplasts of *E. coli* strain MG1655 pFX40 suspended in liquid. (*A*) Phase contrast. (*B*) CL-NAO (red). (*C*) MinD-YFP (green). (*D*) DNA-DAPI (blue).

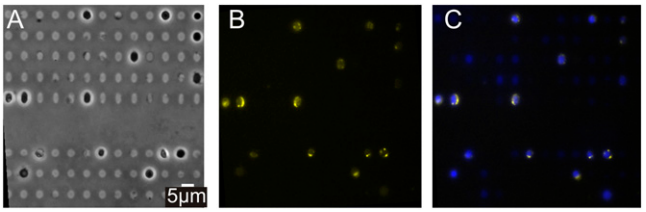

Fig. S8. MinD localization in spheroplasts of *E. coli* JW1241 Δ*cls* pFX40 (YFP-MinD) in microchambers. (*A*) Phase contrast. (*B*) Epifluorescence image of MinD-YFP (yellow false color). (*C*) Merge of MinD-YFP (false-colored yellow) and DNA (DAPI, false-colored blue).

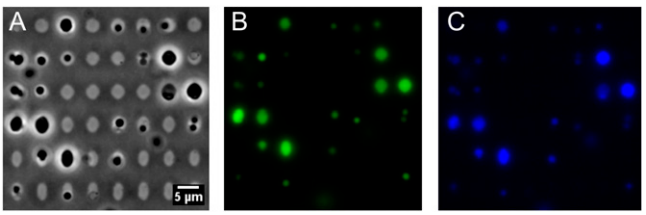

Fig. S9. Images of the distribution of constitutively cytoplasmic eGFP in spheroplasts of *E. coli* MG1655 confined in microchambers demonstrate the homogeneous distribution of a protein that is not localized via membrane curvature: (*A*) Phase-contrast image. (*B* and *C*) Epifluorescence images of (*B*) EGFP (false-colored green) and (*C*) DNA (false-colored blue).

Table S1. Calculation of microchamber volumes

Microchamber curvature (μm^{-1})	Microchamber volume (μm^3)
0.67	26.8
0.73	22.2
1.03	22.6
1.25	23.8
1.56	21.1
2.08	22.8

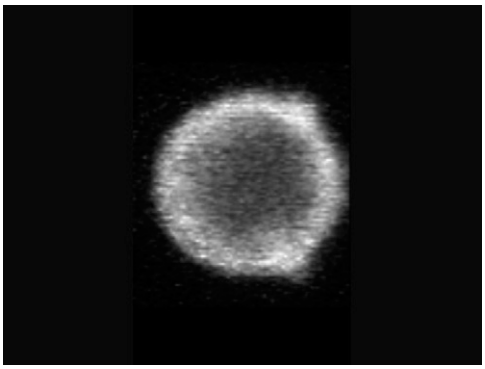

Movie S1. 3D reconstruction of a representative spheroplast in a spherical microchamber labeled with FM 4–64 and imaged using LSCM.

Movie S1

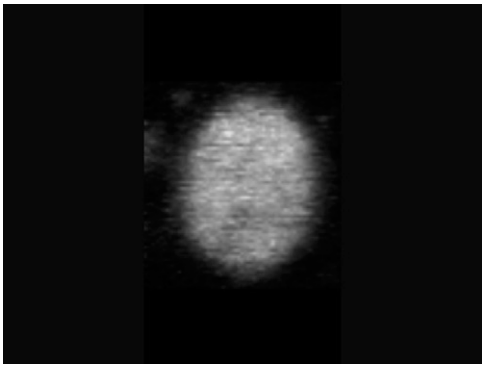

Movie S2. 3D reconstruction of a confocal measurement of a representative spheroplast in a rod-shaped microchamber labeled with FM 4–64 and imaged using LSCM.

Movie S2